$(\vec{d}, t)$ and $(\vec{d}, {}^3\mathrm{He})$ reactions on ^{12}C, ^{16}O, ^{24}Mg, and ^{40}Ca at 29 MeV*

J. D. Cossairt, S. B. Talley, D. P. May, and R. E. Tribble†
Cyclotron Institute, Texas A&M University, College Station, Texas 77843

R. L. Spross
Department of Physics, University of Southwestern Louisiana, Lafayette, Louisiana 70504

(Received 24 January 1978)

The $(\vec{d},t)$ and $(\vec{d}, {}^3\mathrm{He})$ reactions on targets of ^{12}C, ^{16}O, ^{24}Mg, and ^{40}Ca leading to prominent low-lying analog states in the residual nuclei have been studied by measuring differential cross sections and vector analyzing powers. The cross section angular distributions at best exhibit only a weak sensitivity to the transferred angular momentum while the vector analyzing powers are strongly sensitive to the transferred angular momentum and provide a useful signature of the j transfer. Zero-range distorted-wave Born-approximation predictions describe the $\sigma(\theta)$ angular distributions quite well for the lighter targets while they only partially succeed in describing the $A_y(\theta)$ for the lighter targets. An improved distorted-wave Born-approximation description was obtained for the ^{40}Ca target. Some sensitivity to the choice of optical parameters in the distorted-wave Born-approximation analysis, particularly obvious in the $A_y(\theta)$ predictions was seen. Values of extracted spectroscopic factors were generally consistent with those reported in other work (both experimental and theoretical).

[NUCLEAR REACTIONS ^{12}C, ^{16}O, ^{24}Mg, $^{40}Ca(\vec{d}, t)$ and $(\vec{d}, {}^3\mathrm{He})$, $E = 29$ MeV analog states, measured $\sigma(\theta)$ and $A_y(\theta)$, DWBA calculations.]

I. INTRODUCTION

The (d, t) and $(d, {}^3\mathrm{He})$ reactions have proven quite useful in the study of analog states. In the absence of Coulomb effects, the reaction cross sections to analog final states are related by isospin Clebsch-Gordan coefficients since the spectroscopic factors are identical. Of course charge-dependent effects arising both in the exit-channel kinematics and Q-value differences destroy the simple prediction. Several groups have studied (d, t) and $(d, {}^3\mathrm{He})$ reactions on self-conjugate target nuclei.[1-5] In general, standard distorted-wave Born-approximation (DWBA) calculations have been able to account for transitions to analog final states by predicting identical spectroscopic factors to a level of 10–15%, even for cross section differences of more than a factor of 2. The ability of the DWBA predictions to account for the simple Coulomb effects has been exploited to measure charge dependent matrix elements via comparisons of (d, t) and $(d, {}^3\mathrm{He})$ spectroscopic factors in $A = 8$ (Ref. 6), $A = 12$ (Ref. 7), and $A = 16$ (Ref. 8). In all of the cases studied, the j transfer to the final states was not unique. Thus the assumption that the j transfer to analog and antianalog states are identical has been invoked. Of course a direct determination of the j transfer would remove the necessity for this assumption and thereby significantly improve the extraction of a charge-dependent matrix element. Measurements of the vector analyzing power, $A_y(\theta)$, from $(\vec{d}, t)$ and $(\vec{d}, {}^3\mathrm{He})$ reactions represent a possible tool for such a determination.[9]

Very little is known about the j dependence of $A_y(\theta)$. Measurements from ^{208}Pb have demonstrated a characteristic shape for a given j transfer.[10] Also Ludwig *et al.*, using a 15-MeV beam of polarized deuterons, found that the $A_y(\theta)$ was essentially the same for analog states from the $1p$ shell targets ^{10}B and ^{14}N while for an ^{16}O target they observed a significant difference in the ground state transitions.[11] In the present work we have studied the (d, t) and $(d, {}^3\mathrm{He})$ reactions for self-conjugate p and sd shell targets ^{12}C, ^{16}O, ^{24}Mg, and ^{40}Ca. The primary objectives were to determine the sensitivity of $A_y(\theta)$ to the j transfer, to observe the magnitude of Coulomb induced shifts in $A_y(\theta)$ for analog final states, and to test the ability of DWBA calculations to describe the results.

II. EXPERIMENTAL PROCEDURE

Vector polarized deuterons were obtained from an atomic beam ion source and accelerated to 29 MeV by the Texas A&M University 224-cm cyclotron. The beam was energy analyzed and focused onto solid targets at the center of an Ortec 76.2-cm scattering chamber. Natural targets

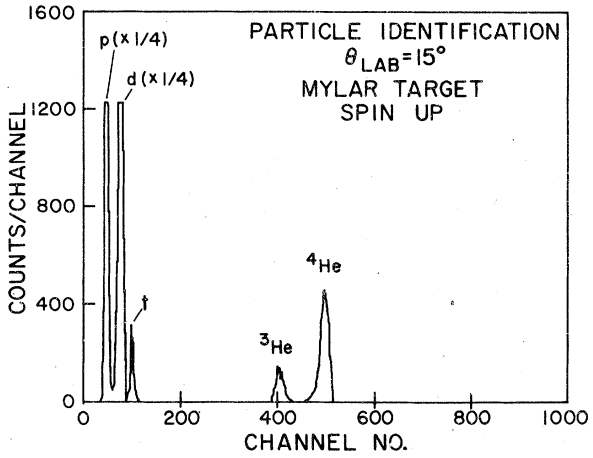

FIG. 1. Typical particle identification spectrum showing results of the range-table look-up procedure.

were used for ^{12}C (0.40 mg/cm^2), ^{16}O (Mylar-0.60 mg/cm^2), and ^{40}Ca (1.1 mg/cm^2), while an isotopic foil was used for ^{24}Mg (1.1 mg/cm^2, 99% ^{24}Mg). Target thicknesses were determined to a precision of ≈10% by measuring the energy loss of alpha particles from an ^{241}Am source. The ^{24}Mg target thickness was also determined by weighing. Symmetric particle detector telescopes, consisting of ΔE, E, and veto Si solid-state detectors, were placed to the left and right of the incident beam direction. Particle identification was accomplished via a range table look-up method by an on-line PDP-15 computer. A typical particle identification spectrum is shown in Fig. 1. Windows were placed around the t and ^{3}He groups and these data were sorted into energy spectra which were subsequently written on magnetic tape for off-line analysis. In both detector telescopes, additional windows were placed just below the t window to insure that no tritons were lost. The detector geometrical solid angle was 1.237 msr corresponding to a $\Delta\theta$ of 2.27°. The particle energy resolution was limited for all targets by kinematic broadening, detector and electronic noise, beam energy spread, and target energy loss. In all cases the resolution was better than 350 keV full width at half maximum (FWHM). Typical energy spectra are shown in Fig. 2.

Approximately 1 m downstream from the main scattering chamber was located a polarimeter chamber containing a carbon target. The ^{12}C($\vec{d}$, α)^{10}B reaction was used as a polarization monitor following the results reported by Cossairt *et al.*[12] As explained in Ref. 12, single detectors were adequate for use in the polarimeter chamber. For the present experiment, the polarimeter detectors were placed at a laboratory scattering angle of 65°. At this angle the analyzing power for the ^{10}B ground state transition is ≈0 while that of the first excited state is ≈0.85. Thus these two states provide an excellent monitor of both the beam polarization and polarimeter instrumental asymmetries. The beam spot size in the polarimeter chamber was defined by an upstream collimator in order to limit the energy spread due to kinematic broadening. A carbon Faraday cup was an integral part of the polarimeter chamber. Also, the entire polarimeter chamber, including the beam defining collimator, was electrically isolated and shorted to the Faraday cup. As an additional check, the beam polarization was measured by a ^{4}He gas polarimeter at the beginning of an experiment as an independent calibration for the ^{12}C polarimeter. The average beam polarization was 50.5% (with ~3% variations) and the on target beam current was maintained between 20 and 60 nA.

In all cases, two sets of spectra were taken at each angle corresponding to the two possible spin orientations of the beam. The yields obtained from the four spectra determined both the differential cross section and vector analyzing power. Absolute cross sections are estimated to be accurate to 20% due to uncertainties in target thicknesses, beam integration, and experimental geometry. Throughout this work the definitions of the "Madison Convention" of 1970 (Ref. 13) are used. The vector analyzing power is always discussed in terms of A_y, its value in Cartesian coordinates.

III. DWBA CALCULATIONS

DWBA calculations for both differential cross sections and analyzing powers were performed with the computer code DWUCK4.[14] The optical potentials which were used are listed in Table I. In the entrance channel the parameters were taken from Perrin *et al.*[15] who fitted elastic vector analyzing powers as well as differential cross sections. Other deuteron parameters were tried with very small differences in the results. In the exit channel, the calculations were sensitive to different sets of parameters. This effect was most noticeable in the calculations of vector analyzing powers. The global parameter set of Becchetti and Greenlees[16] (denoted as set A in Table I) and parameters modified slightly from those of Gaillard *et al.*[1] (denoted as set B in Table I) were both used in the analysis presented in this paper. These two parameter sets give generally equivalent elastic scattering cross sections. The calculations were only very weakly sensitive to the

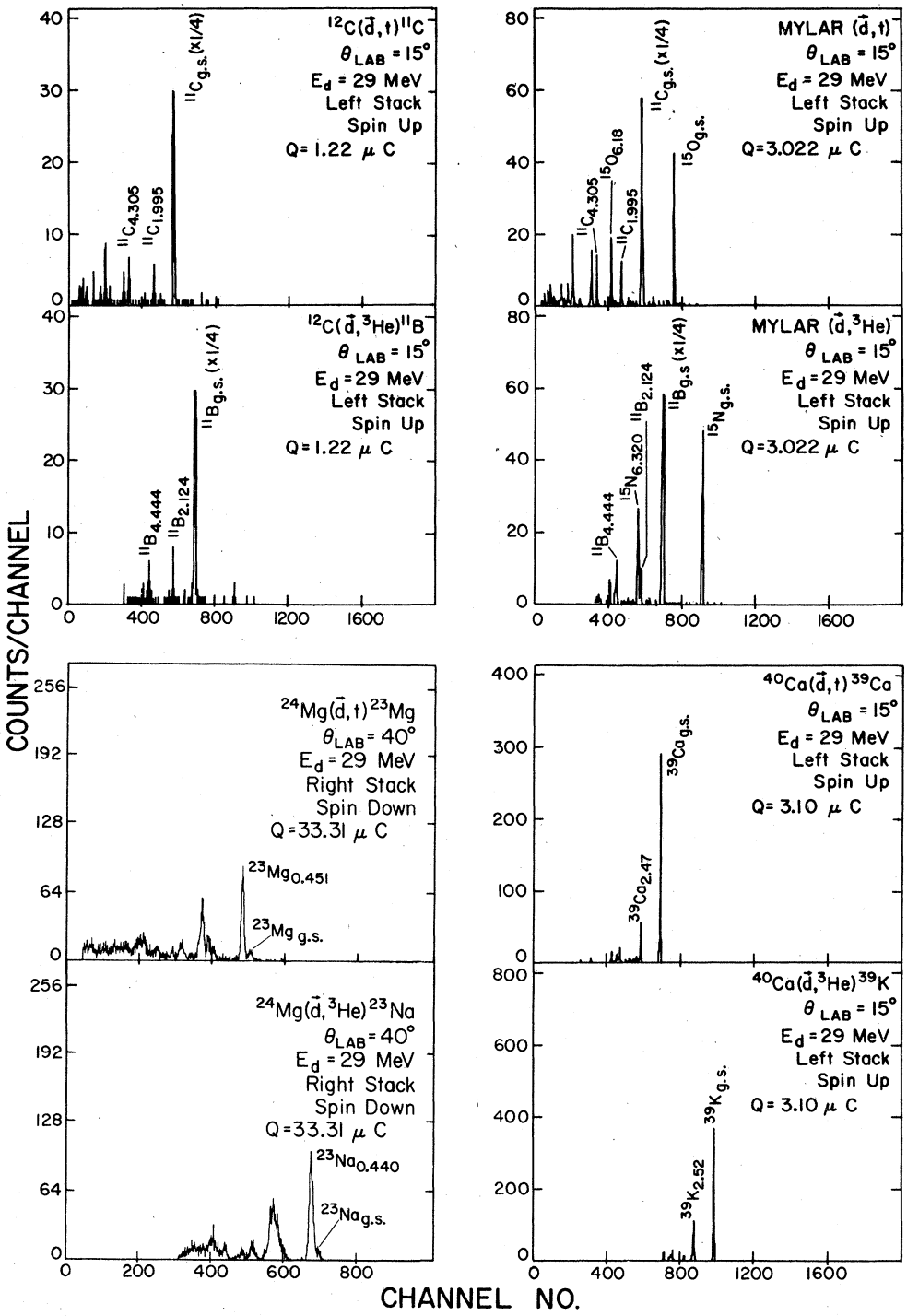

FIG. 2. Sample spectra for $(\vec{d},t)$ and $(\vec{d},{}^3\mathrm{He})$ reactions identifying the laboratory scattering angle, left or right stack, beam spin orientation, and integrated beam current.

addition of spin-orbit terms in the exit channel optical potentials.

Single-particle wave functions were calculated assuming the transferred nucleon to be bound in a real Woods-Saxon potential having radius and diffuseness parameters of 1.25 and 0.65 fm, respectively. A Thomas spin-orbit λ factor of 25 was included in the form factor. The depth of the

binding potential was constrained to reproduce the physical separation energy. Quantum numbers nlj of the transferred nucleon were determined in the usual manner from angular momentum and shell model considerations. Of course, for the even-even self-conjugate targets considered in the present work, these quantum numbers are unique for a given final state in the residual nucleus assuming a one-step direct reaction mechanism. In the calculations, both finite-range corrections (using the Hulthén form in local energy approximation) and nonlocal corrections were made to the form factor using the parameters of Kunz.[14] The calculated predictions of $\sigma(\theta)$ were not significantly sensitive to these corrections while the $A_y(\theta)$ were only weakly sensitive to them, the main effect there being to smooth out extreme oscillations in the calculated values.

Spectroscopic factors C^2S were extracted using the normalization of Hering[17]:

$$\left(\frac{d\sigma}{d\Omega}\right)_{\text{exp}} = \frac{NC^2S}{2j+1}\,\sigma_{\text{DWUCK}},$$

with $N(d, t) = 2.54$ and $N(d, {}^3\text{He}) = 2.28$ where C^2 is the usual isospin Clebsch-Gordan coefficient ($=\frac{1}{2}$). For consistency the spectroscopic factors were evaluated at the first observed maxima in the angular distributions which occur near 40° c.m. for all targets considered.

IV. RESULTS

Experimental angular distributions are compared to the DWBA calculations in Figs. 3–6. The fits

TABLE I. Optical model parameters:

$$V(r) = V_c(r) - V(e^x + 1)^{-1} - i\,W_{IV}(e^{x'} + 1)^{-1} + 4i\,W_{ID}\,\frac{d}{dx'}(e^{x'} + 1)^{-1} + \left(\frac{\hbar}{m_\pi c}\right)^2 V_{L\cdot S}\,\frac{1}{r}\,\frac{d}{dr}\,(e^{x''} + 1)^{-1}\,L\cdot S,$$

$$x = (r - r_V A^{1/3})/a_v, \quad x' = (r - r_I A^{1/3})/a_I, \quad x'' = (r - r_{L\cdot S} A^{1/3})/a_{L\cdot S}.$$

	V (MeV)	r_V (fm)	a_V (fm)	W_{IV} (MeV)	W_{ID} (MeV)	r_I (fm)	a_I (fm)	$V_{L\cdot S}$ (MeV)	$r_{L\cdot S}$ (fm)	$a_{L\cdot S}$ (fm)
Entrance channel										
$d + {}^{12}\text{C}, {}^{16}\text{O}$	86.0	1.13	0.697		8.62	1.48	0.72	8.22	0.854	0.685
$d + {}^{24}\text{Mg}$	87.1	1.13	0.82		13.00	1.325	0.75	4.66	0.960	0.465
$d + {}^{40}\text{Ca}$	93.0	1.13	0.800		10.23	1.390	0.75	5.07	0.900	0.562
Exit channel set A										
$t + {}^{11}\text{C}$	162.9	1.2	0.72	50.796		1.4	0.88			
${}^3\text{He} + {}^{11}\text{B}$	153.3	1.2	0.72	39.65		1.4	0.88			
$t + {}^{15}\text{O}$	161.23	1.2	0.72	46.85		1.4	0.88			
${}^3\text{He} + {}^{15}\text{N}$	151.33	1.2	0.72	37.05		1.4	0.88			
$t + {}^{23}\text{Mg}$	162.1	1.2	0.72	41.21		1.4	0.88			
${}^3\text{He} + {}^{23}\text{Na}$	150.1	1.2	0.72	39.06		1.4	0.88			
$t + {}^{39}\text{Ca}$	161.82	1.2	0.72	42.34		1.4	0.88			
${}^3\text{He} + {}^{39}\text{K}$	148.64	1.2	0.72	34.02		1.4	0.88			
Exit channel set B										
$t + {}^{11}\text{C}$ ${}^3\text{He} + {}^{11}\text{B}$	160.5	1.4	0.626	17.6		1.9	0.626			
$t + {}^{15}\text{O}$ ${}^3\text{He} + {}^{15}\text{N}$	180.0	1.086	0.782	15.5		2.12	0.467			
$t + {}^{23}\text{Mg}$ ${}^3\text{He} + {}^{23}\text{Na}$	160.0	1.1	0.720	14.8		1.9	0.58			
$t + {}^{39}\text{Ca}$ ${}^3\text{He} + {}^{39}\text{K}$	161.8	1.17	0.71	12.1		1.89	0.846			

TABLE II. Experimental and theoretical spectroscopic factors C^2S. Bombarding energies are given for each experimental determination; TH denotes theoretical calculation; (a) present work, listing results obtained with parameter sets A and B; (b) Gaillaird *et al.*, Ref. 1; (c) Nelson and Roberson, Ref. 4; (d) Firestone *et al.*, Ref. 18; (e) Hinterberger *et al.*, Ref. 2; (f) Hiebert *et al.*, Ref. 19, NL indicates nonlocal corrections used and FR indicates finite-range corrections used; (g) Purser *et al.*, Ref. 3; (h) Doubre *et al.*, Ref. 20 (with nonlocal and finite-range corrections); (i) Wagner *et al.*, Ref. 21; (j) Kramer *et al.*, Ref. 22; (k) Arditi *et al.*, Ref. 23; (l) Cohen and Kurath, Ref. 24; (m) Wildenthal, as quoted in Ref. 4; (n) Ellis and Engeland weak coupling model, Ref. 18.

State	J^π	a A	29.0 B	b 28.0	c 21.1	d 29.0	e 52.0	f FR	34.4 NL	g 20.0	h 82.0	i 52.0	j 52.0	k 80.0	l TH	m TH	n TH
$^{11}C_{g.s.}$	$\frac{3}{2}^-$	3.97	2.82	2.76											2.85		
$^{11}B_{g.s.}$	$\frac{3}{2}^-$	4.42	3.22	2.44			2.98								2.85		
$^{15}O_{g.s.}$	$\frac{1}{2}^-$	2.50	2.25	1.29						1.50							1.51
$^{15}N_{g.s.}$	$\frac{1}{2}^-$	2.17	2.34	1.22		2.60		2.14	1.87	2.10	2.80						1.51
$^{15}O_{6.2}$	$\frac{3}{2}^-$	3.34	3.28							3.10							2.9
$^{15}N_{6.3}$	$\frac{3}{2}^-$	2.81	3.68			5.60		3.72	3.32		3.40						2.9
$^{23}Mg_{g.s.}$	$\frac{3}{2}^+$	0.07	0.08		0.33											0.08	
$^{23}Na_{g.s.}$	$\frac{3}{2}^+$	0.08	0.09		0.26								0.24	0.47		0.08	
$^{23}Mg_{0.4}$	$\frac{5}{2}^+$	0.57	0.63		2.20											2.73	
$^{23}Na_{0.4}$	$\frac{5}{2}^+$	0.47	0.70		2.10								3.78	2.90		2.73	
$^{39}Ca_{g.s.}$	$\frac{3}{2}^+$	4.85	4.07	5.35													
$^{39}K_{g.s.}$	$\frac{3}{2}^+$	5.03	4.66	3.93				4.23	3.53		3.60	3.70					
$^{39}Ca_{2.5}$	$\frac{1}{2}^+$	1.26	1.06														
$^{39}K_{2.5}$	$\frac{1}{2}^+$	1.05	0.86					1.62	1.35		1.10	1.33					

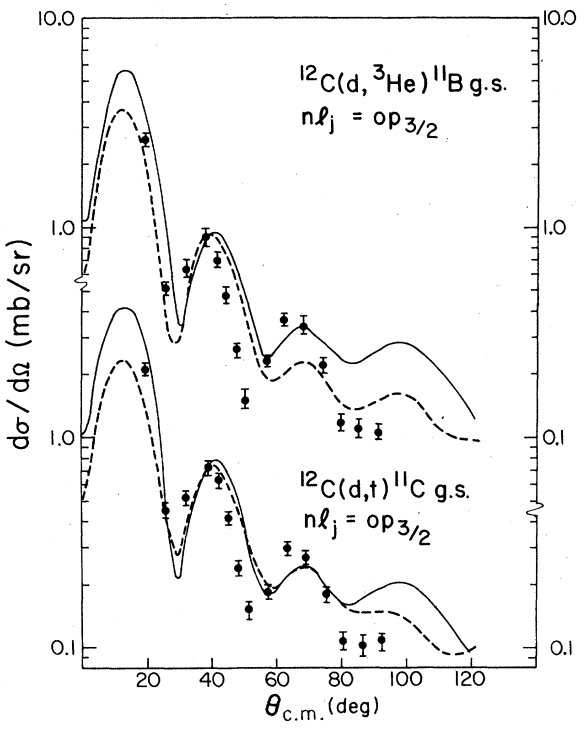

FIG. 3. Angular distributions for ^{12}C(d,t) ^{11}C and ^{12}C$(d,{}^{3}\mathrm{He})$ ^{11}B reactions. The quantum numbers nlj of the transferred nucleon are given. Results of parameter set A are shown as a solid line while those of set B are shown as a dashed line.

in general are acceptable, especially at the more forward angles. The general features observed in the angular distributions have been noted from other measurements obtained with unpolarized beams (e.g., Ref. 1). Qualitatively the analog states show similar angular distributions. However with increasing nucleon number A, Coulomb effects shift the diffraction patterns and enhance the $(d,{}^{3}\mathrm{He})$ to (d,t) cross section ratio. A detailed accounting of these Coulomb induced shifts has been given in Ref. 5. We also note essentially no discernible j dependence in the angular distributions. This is apparent in the $A=15$ and $A=23$ final states where both $j=l\pm\frac{1}{2}$ states have been observed.

In view of the emphasis of the present work, spectroscopic factors have been extracted primarily as a check of the consistency of the data. In all cases data have not been obtained at forward angles where reliable spectroscopic factors can be determined. Table II displays the results for the spectroscopic factors found in the present work with results quoted for both optical parameter sets A and B. Also included in the table

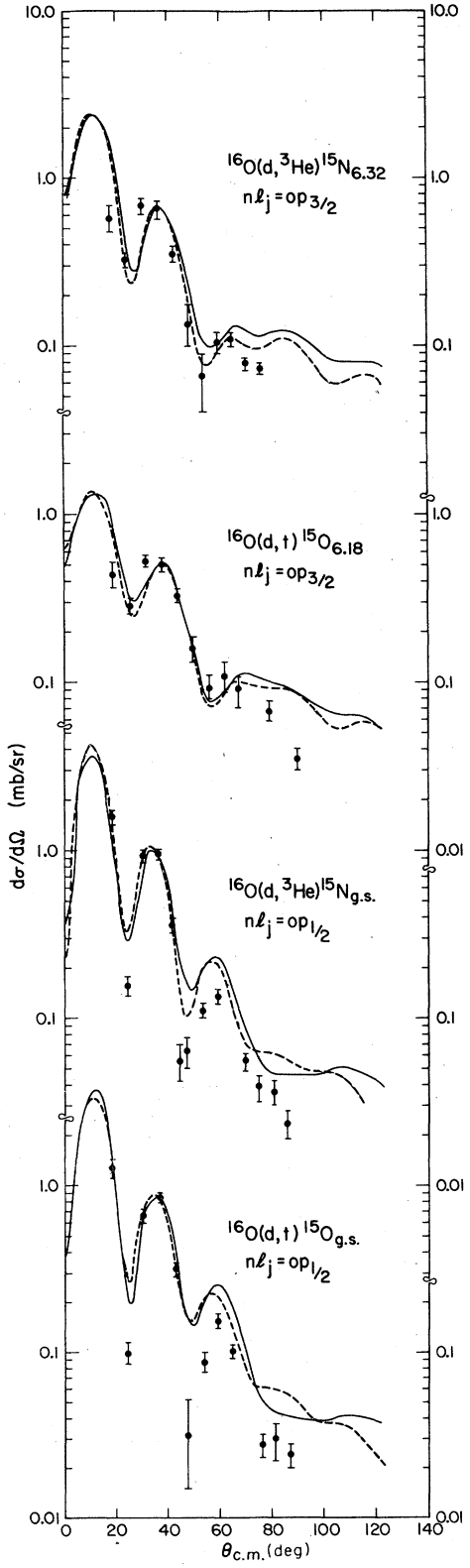

FIG. 4. Angular distributions for ^{16}O(d,t) ^{15}O and ^{16}O$(d,{}^{3}\mathrm{He})$ ^{11}B (same notation as Fig. 3).

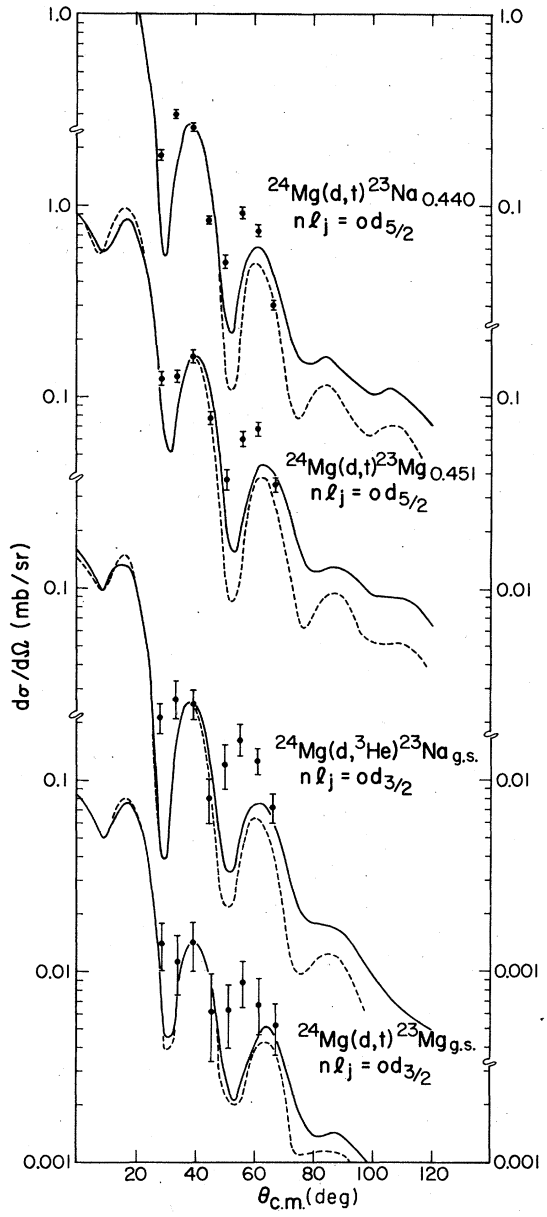

FIG. 5. Angular distributions for $^{24}\mathrm{Mg}(d,t)$ $^{23}\mathrm{Mg}$ and $^{24}\mathrm{Mg}(d, {}^3\mathrm{He})$ $^{23}\mathrm{Na}$ reactions (same notation as Fig. 3).

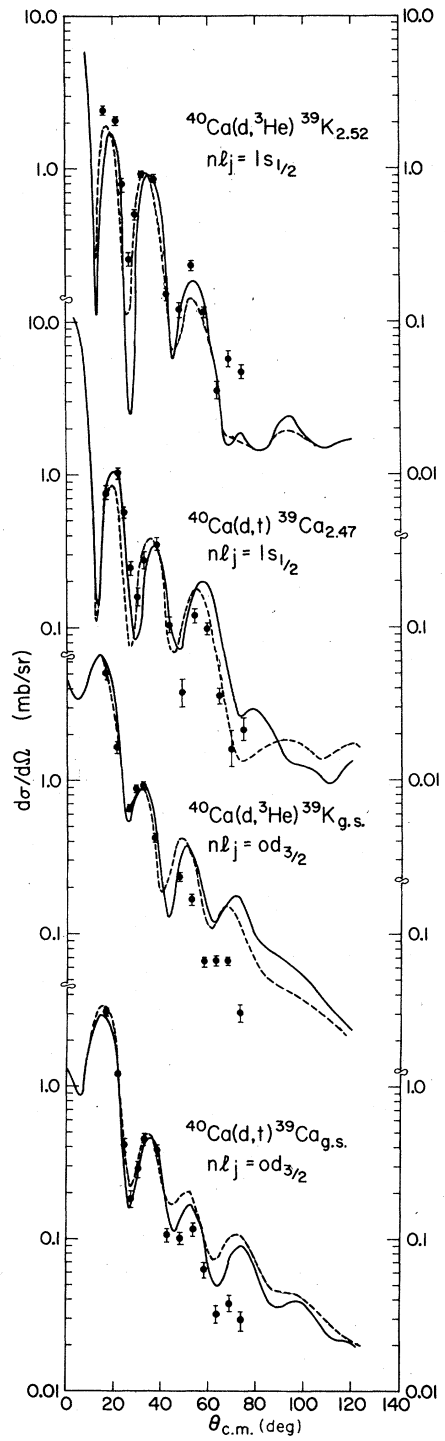

FIG. 6. Angular distributions for $^{40}\mathrm{Ca}(d,t)$ $^{39}\mathrm{Ca}$ and $^{40}\mathrm{Ca}(d, {}^3\mathrm{He})$ $^{39}\mathrm{K}$ reactions (same notation as Fig. 3).

are other experimental determinations and shell model predictions. The agreement between the $C^2S(d,t)$ and $C^2S(d, {}^3\mathrm{He})$ for analog states is quite good, generally showing consistency at the 10–15% level. In most cases the absolute C^2S are also in good agreement with other experimental and also theoretical predictions. A notable exception is the C^2S for $\frac{5}{2}^+$ states in $A = 23$. The discrepancy in this case is likely due to the lack of forward angle data. In a similar experiment at a lower energy,[4] the DWBA prediction for the second maximum (where the present normalization is taken) underestimates the data by more than a factor of 2. Also this effect was observed for transitions to $\frac{5}{2}^+$ levels in $A = 27$.[5]

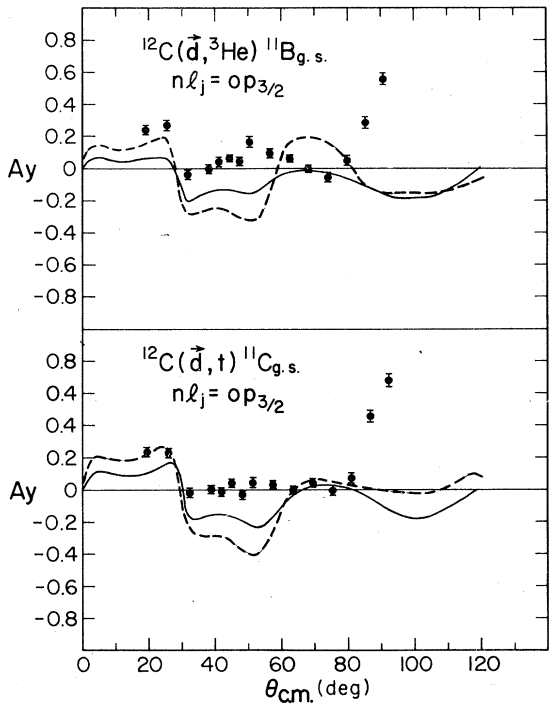

FIG. 7. A_y angular dependence for $^{12}C(\vec{d},t)\ ^{11}C$ and $^{12}C(\vec{d},\ ^3He)\ ^{11}B$ reactions (same notation as Fig. 3).

In Figs. 7–10 the vector analyzing power data and DWBA predictions are displayed. The results are somewhat similar to those observed for the cross sections. That is, the data for the two reaction exit channels generally agree with each other for transitions to analog states. However as the nuclear number increases, Coulomb effects again cause changes in A_y for the (d, t) and $(d, {}^3\mathrm{He})$ transitions. The DWBA predictions, which are also included in the figures, are generally in poor agreement with the data, except for the heavier target ^{40}Ca.

The present results show clearly that there is a significant j dependence in the shape of the $A_y(\theta)$. This is especially apparent for the ^{16}O and ^{24}Mg targets where direct comparisons between different j transfers having the same value of l can be made for the same target nucleus. The $j = \frac{3}{2}$ transitions from the ^{12}C target are only suggestive, however, of those from the ^{16}O target. This result indicates that the characteristic shape for each j transfer is dependent upon the specific target nucleus involved. This same target dependence is also seen in the case of the $j = \frac{3}{2}$ transitions from the ^{24}Mg and ^{40}Ca targets. In fact, the $j = \frac{5}{2}$ transition from ^{24}Mg strongly resembles the $j = \frac{3}{2}$ transition from ^{40}Ca. It thus appears that the use of these reactions to identify unknown j transfers

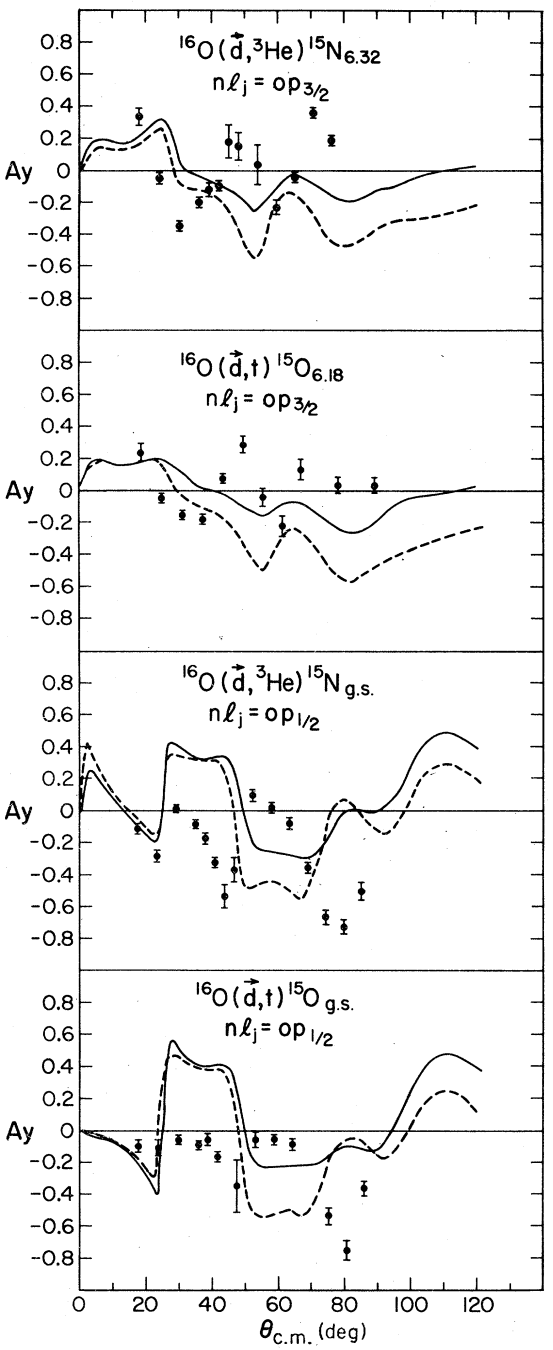

FIG. 8. A_y angular dependence for $^{16}O(\vec{d},t)\ ^{15}O$ and $^{16}O(\vec{d},\ ^3He)\ ^{15}N$ reactions (same notation as Fig. 3).

is questionable unless known j transfers from the target of interest are available for purposes of comparison. This differs from the conclusion of Bechtold *et al.* drawn from an analysis of their data for $(d, {}^3\mathrm{He})$ reactions on targets of

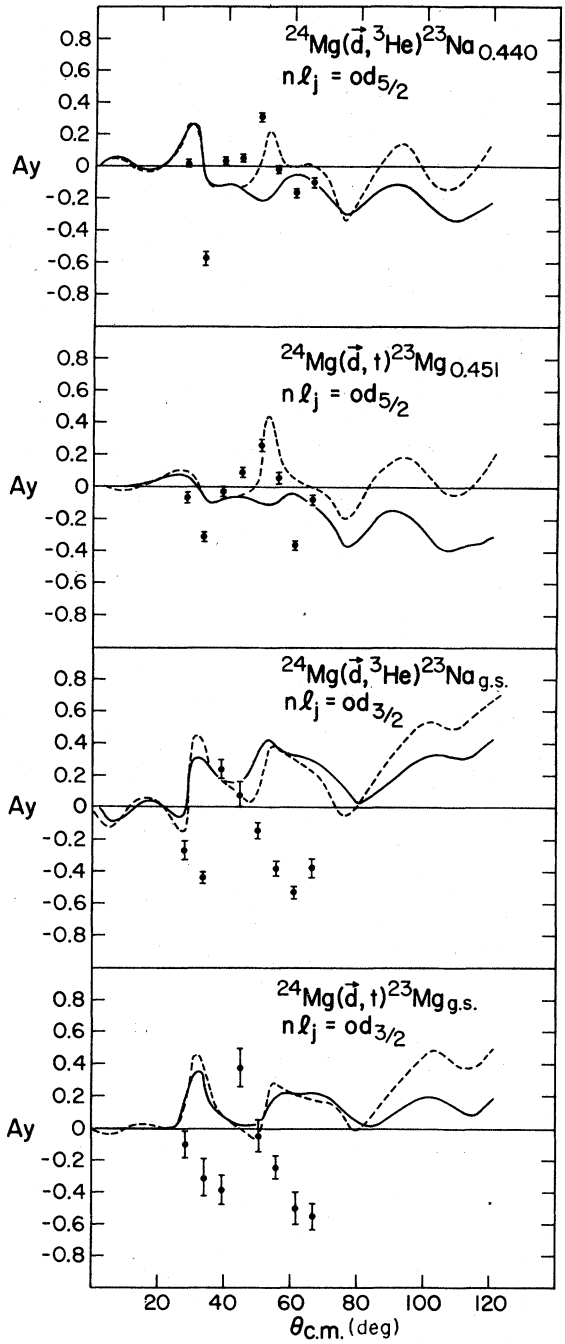

FIG. 9. A_y angular dependence for ^{24}Mg($\vec{d},t$) ^{23}Mg and ^{24}Mg($\vec{d}$, ^{3}He) ^{23}Na reactions (same notation as Fig. 3).

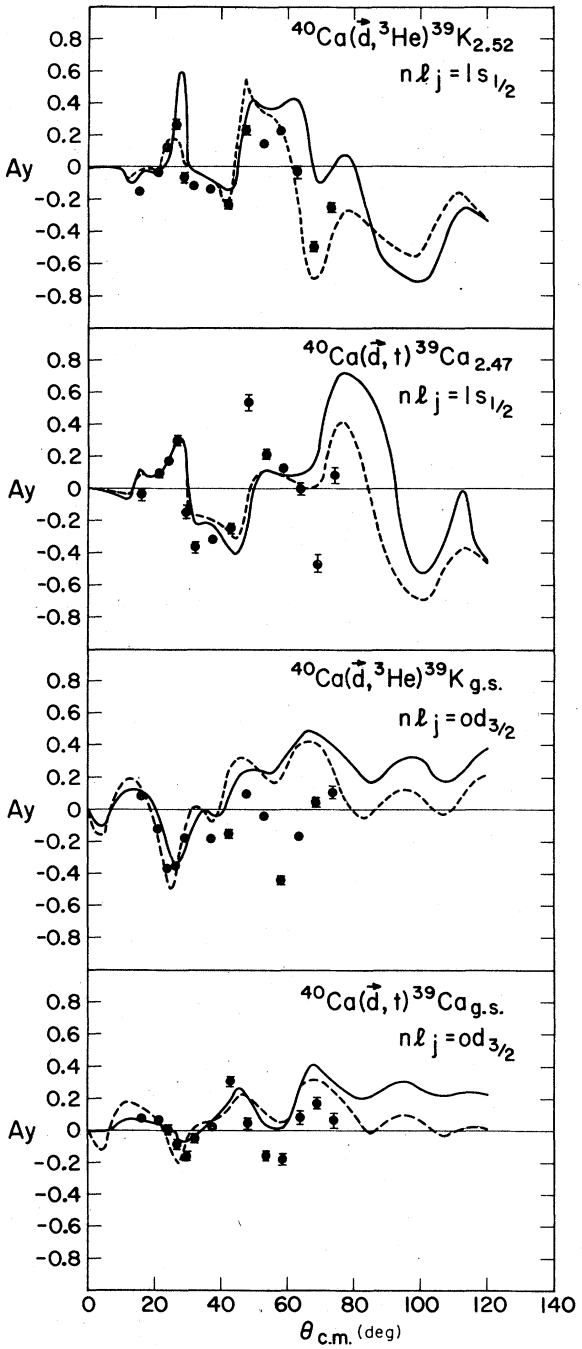

FIG. 10. A_y angular dependence for ^{40}Ca($\vec{d},t$) ^{39}Ca and ^{40}Ca($\vec{d}$, ^{3}He) ^{39}K reactions (same notation as Fig. 3).

^{16}O, ^{28}Si, and ^{40}Ca at 52 MeV.[25] However, their data do exhibit some mass and Q-value dependence; though weaker than that observed in the present work. It is very encouraging that the characteristic j dependence is essentially the same for both the (d,t) and $(d,{}^3\mathrm{He})$ reaction channels as the study of such transfer reactions with vector polarized beams represents a new probe of analog states which may be sensitive to effects not revealed by the cross section alone. Also the strong j dependence exhibited even for the light targets indicates that a measurement of $A_y(\theta)$ can

help reveal the structure of states that are assumed to be analog, antianalog pairs.

V. SUMMARY

The $(\vec{d}, t)$ and $(\vec{d}, {}^3\mathrm{He})$ reactions on self-conjugate p and sd shell targets to analog states have essentially identical angular distribution shapes and very similar $A_y(\theta)$ for all cases studied in the present work. A significant j dependence of the $A_y(\theta)$ data was obtained for transitions having the same orbital angular momentum while in such cases the cross section angular distributions were essentially identical. This j dependence, however, has a shape dependent upon the target nucleus involved. Zero-range DWBA calculations were able to describe the shapes of the angular distributions quite adequately and yielded spectroscopic factors generally reasonable in view of other experimental and theoretical work. The description of $\sigma(\theta)$ improved with increasing mass number. The calculations were only crudely able to describe the $A_y(\theta)$ for the lighter targets while giving an improved description for the ^{40}Ca target; a feature which perhaps points out difficulties involved with such DWBA calculations for transfer reactions on light nuclei. The strong j dependence of $A_y(\theta)$ exhibited in the present data clearly demonstrates the usefulness of analyzing power measurements for studies of analog states.

We would like to thank the Cyclotron Institute staff for their assistance throughout this work. Special thanks are due R. York for his help with the polarized ion source. We acknowledge the help of D. Tanner and K. Jennings with the data acquisition and reduction.

---

*Supported in part by the National Science Foundation and the Robert A. Welch Foundation.

†Alfred P. Sloan Fellow.

[1]M. Gaillard, R. Bouché, L. Feuvrais, P. Gaillard, A. Guichard, M. Gusakow, J. L. Leonhardt, and J.-R. Pizzi, Nucl. Phys. A119, 161 (1968).

[2]F. Hinterberger, G. Mairle, U. Schmidt-Rohr, P. Turek, and G. J. Wagner, Nucl. Phys. A106, 161 (1968).

[3]K. H. Purser, W. P. Alford, D. Cline, H. W. Fulbright, H. E. Gove, and M. S. Krick, Nucl. Phys. A132, 75 (1969).

[4]R. O. Nelson and N. R. Roberson, Phys. Rev. C 6, 2153 (1972).

[5]R. E. Tribble and K.-I. Kubo, Nucl. Phys. A282, 269 (1977).

[6]M. A. Oothoudt and G. T. Garvey, Nucl. Phys. A284, 41 (1977).

[7]J. M. Lind, G. T. Garvey, and R. E. Tribble, Nucl. Phys. A276, 25 (1977).

[8]G. J. Wagner, K. T. Knöpfle, G. Mairle, P. Doll, H. Hofner, and J. L. C. Ford, Jr., Phys. Rev. C 16, 1271 (1977).

[9]D. P. Balamuth (private communication).

[10]B. Mayer, H. E. Conzett, W. Dahme, D. G. Kovar, R. M. Larimer, and Ch. Leemann, Phys. Rev. Lett. 32, 1452 (1974).

[11]E. J. Ludwig, C. E. Busch, T. B. Clegg, S. K. Datta, and A. C. Watkins, Nucl. Phys. A230, 271 (1974).

[12]J. D. Cossairt, W. S. Burns, and R. A. Kenefick, Nucl. Phys. A287, 13 (1977).

[13]in *Proceedings of the Third International Symposium on Polarization Phenomena in Nuclear Reactions, Madison, Wisconsin, 1970,* edited by H. H. Barschall and W. Haeberli (Univ. of Wisconsin Press, Madison, 1971).

[14]P. D. Kunz, University of Colorado report, 1975 (unpublished).

[15]G. Perrin, N. V. Sen, J. Arvieux, R. Darves-Blanc, J. L. Durand, A. Fiore, J. C. Gondrand, F. Merchez, and C. Perrin, Nucl. Phys. A282, 221 (1977).

[16]F. D. Becchetti and G. W. Greenless, Ref. 13, p. 682.

[17]W. R. Hering, H. Becker, C. A. Wiedner, and W. J. Thompson, Nucl. Phys. A151, 33 (1970).

[18]M. A. Firestone, J. Jänecke, A. Dudek-Ellis, P. J. Ellis, and T. Engeland, Nucl. Phys. A258, 317 (1976).

[19]J. C. Hiebert, E. Newman, and R. H. Bassel, Phys. Rev. 154, 898 (1967).

[20]H. Doubre, D. Royer, M. Arditi, L. Bimbot, N. Frascaria, J. P. Garron, and M. Riou, Phys. Lett. 29B, 355 (1969).

[21]G. J. Wagner, P. Doll, K. T. Knöpfle, and G. Mairle, Phys. Lett. 57B, 413 (1975).

[22]E. Kramer, G. Mairle, and G. Kaschl, Nucl. Phys. A165, 353 (1971).

[23]M. Arditi, L. Bimbot, H. Doubre, N. Frascaria, J. P. Garron, M. Riou, and D. Royer, Nucl. Phys. A165, 129 (1971).

[24]S. Cohen and D. Kurath, Nucl. Phys. A101, 1 (1967).

[25]V. Bechtold, L. Friedrich, P. Doll, K. T. Knöpfle, G. Mairle, and G. J. Wagner, Phys. Lett. 72B, 169 (1977).